J. Fluid Mech. (1981), *vol.* 109, *pp.* 435–463
Printed in Great Britain

Evolution and breakdown of a vortex street in two dimensions

By HASSAN AREF† AND ERIC D. SIGGIA
Laboratory of Atomic and Solid State Physics, Clark Hall,
Cornell University, Ithaca, NY 14853, USA

(Received 2 June 1980 and in revised form 7 November 1980)

The initial-value problem defined by two parallel vortex sheets of opposite sign is studied. Strictly two-dimensional, incompressible, nearly inviscid dynamics is assumed throughout. The roll-up of the sheets into a vortex street is simulated numerically using 4096 point vortices. Much longer runs than in previous work are performed, and it is found that only for a finite range of values of the ratio, h/λ, of sheet separation to perturbation wavelength, does a long-lived vortex street emerge. For $h/\lambda \gtrsim 0{\cdot}6$ a pairing transition within each row intervenes. For $h/\lambda \lesssim 0{\cdot}3$ we find oscillatory modes.

Using up to 16384 point vortices, we also study the breakdown of the metastable street to a two-dimensional, turbulent shear flow. The vortex blobs that made up the street may merge with others of the same sign after the breakdown, but otherwise persist throughout the turbulent regime. Neither their disintegration nor amalgamation with vortices of opposite sign was observed. Using dimensional arguments we derive the relevant scaling theory, and show that it applies to a flow started from two random vortex sheets. The resulting turbulence is not self-similar. For the turbulent flow that follows from the breakdown of a regular vortex street two length scales with different power-law growth in time appear to be necessary. The important differences in the asymptotic structure of flows initialized from random and regular sheets leads us to question the idea of universality. The influence of the symmetry of the initial perturbation on the subsequent development is also considered.

1. Introduction

The emergence of a vortex street downstream of a cylinder placed in an oncoming steady flow is among the best-known phenomena of hydrodynamics. This periodic response to a static upstream velocity field defines an initial condition from which the turbulent wake ultimately evolves. In the laboratory the flow becomes substantially three-dimensional after breakdown of the vortex street. In a numerical simulation on the other hand the dynamics can be kept strictly two-dimensional. The vortex structures that made up the street then survive and evolve toward an asymptotic state of surprising dynamical simplicity. In this paper we study the formation and subsequent breakdown of a vortex street in two-dimensional incompressible, nearly inviscid hydrodynamics.

There is a large literature concerned with experiments on vortex shedding from a

† Present address: Division of Engineering, Brown University, Providence, Rhode Island 02912.

bluff body. The early review by Roshko (1954) is still useful as an introduction. The later high-Reynolds-number results of Roshko (1961) are also of interest in connection with the present paper. A review of a recent conference on vortex shedding from bluff bodies has appeared in this journal (Bearman & Graham 1980). This review mentions present trends in the subject and contains several references to earlier work.

The formation of a vortex street by vortex shedding has been simulated numerically using vortex methods by many authors. The random vortex method of Chorin (1973) was subsequently used by Ashurst (1979) to simulate the two-dimensional mixing layer downstream of a splitter plate. For general reviews of vortex methods for flow computation the reader is referred to Clements & Maull (1975), Zabusky (1977), Chorin (1980) and Leonard (1980).

The initial conditions that we consider consist of two vortex sheets of opposite sign discretized into point vortices. The sheets are in a rectangular flow box with periodic boundaries left and right, rigid boundaries top and bottom. A sinusoidal perturbation of small amplitude is imposed on the sheets. When the same perturbation is applied to both sheets, they roll up to produce a staggered array of finite area vortices, the von Kármán vortex street. An early investigation by Abernathy & Kronauer (1962; henceforth referred to as AK) is frequently quoted in connection with this problem. We show here that longer runs with higher spatial resolution substantially alter their conclusions and suggest modes other than street formation. The pairing mechanism originally suggested by Taneda (1959) (see also Durgin & Karlsson 1971), whereby a vortex street doubles its longitudinal scale is seen convincingly for the first time in a numerical simulation.

The breakdown problem has not received much prior attention in the literature. The reason is, as we have already mentioned, that a real vortex street is expected to break down to a fully three-dimensional flow, although experiments by Papailiou & Lykoudis (1974) do suggest that the street vortices persist for some time. Our interest in the purely two-dimensional problem is motivated by several considerations. First of all the corresponding numerical experiment for three-dimensional flow is only barely feasible with present-day computers. Of more interest are certain questions of principle, concerning the validity of simple scaling and universality in the presence of structures in the turbulence, that are equally relevant in two and three dimensions. Such questions are accessible to our computations.

The numerical method used is the vortex-in-cell algorithm described by Christiansen (1973). Our version of the code and certain features of the algorithm were discussed in a previous publication concerned with the two-dimensional shear layer (Aref & Siggia 1980, henceforth referred to as AS). For the initial instability studies we used a small grid (64×64) with a total of 4096 point vortices. The perturbation wavelength was chosen so that four or eight street vortices of either sign emerged. Since the flow pattern under investigation was itself periodic, it was judged admissible to have so few structures within the periodic boundaries. The results obtained for the initial instability are the subject of § 2.

For the study of vortex street breakdown, substantially larger simulations were performed, typically 16384 vortices on a 512×256 grid together with an initial perturbation that resulted in a street with 64 vortex regions of either sign. Runs on the small grid were also done for illustrative purposes. The breakdown of a vortex street leads to a two-dimensional turbulent shear flow. In this flow certain simple, clearly

identifiable modes dominate the dynamics. In § 3 we first describe these modes qualitatively. We then consider the question of scaling of the large-scale statistics such as mean velocity, velocity fluctuation intensities and Reynolds stress. Using dimensional arguments, we derive a scaling theory for this type of flow. The theory contains the growth exponent for the thickness of the turbulent region as a free parameter. Since the simulation conserves both momentum and kinetic energy it turns out that the scaling theory does not describe a statistically self-similar turbulence. In particular, the scaling theory is not the spatial to temporal transcription of the traditional self-preserving plane wake. We check numerically that the scaling we derive is the applicable one in the sense that the transcription just mentioned would lead to secular variations in scaled plots of the average and mean square velocity.

The detailed comparison between the numerical experiment and a one-length scaling theory is less favourable than in the smaller shear layer calculation described in AS. This could simply be due to a higher level of statistical noise because in the present case significant cancellations occur between contributions from vortex regions of different sign. However, the dynamics of the vortex structures in the flow suggests much more interesting possibilities. The simulations indicate that when a vortex street breaks down in two dimensions the resulting flow exhibits two length scales with different power-law growth in time. These are (1) the width of a 'central band' or 'core region' containing positive and negative macro-vortices in equal numbers which expands diffusively, i.e. as $t^{\frac{1}{2}}$ where t is the time, and (2) outside this region a 'gas' of weakly interacting vortex dipoles, neutral vortex pairs that propagate with constant velocity and thus introduce a length scale that increases linearly with time.

Section 4 contains discussion and conclusions. First we produce a kinetic argument to suggest that when a street of point vortices breaks down the momentum thickness must increase as $t^{\frac{1}{2}}$. This represents the slow growth limit of the scaling theory of § 3. Then we investigate the role of the symmetry of the initial perturbation. Throughout §§ 2 and 3 we only consider the case when the two vortex sheets roll up into a staggered array of vortices. In § 4 we examine the roll-up into symmetrically placed vortices. This symmetry is preserved by the equations of motion and the dominant mode now is a pairing of like signed vortices. This flow then resembles the early stages of a plane jet. The thickness grows linearly in time in this case which represents the fastest growth possible in our scaling formulation. These results lead us to discuss briefly the relations between our model flows and real plane wakes and jets.

The nature of the dominant dynamical processes after vortex street breakdown leads us to question the long-term universality of the flow. In particular, if we compare a flow started from uniform vortex sheets with a sinusoidal perturbation with another started from vortex sheets with an irregular distribution of circulation but with the same initial spacing and velocity defect, will the large-scale statistics be identical at long times? We conclude § 4 by relating our observations to previous conjectures of non-universality in two-dimensional turbulence.

2. The initial instability

The linearized stability analysis for two vortex sheets of opposite sign was discussed by AK who pointed out the interesting feature that the growth rates for a symmetric and an antisymmetric perturbation are equal. (This degeneracy is lifted if the sheets

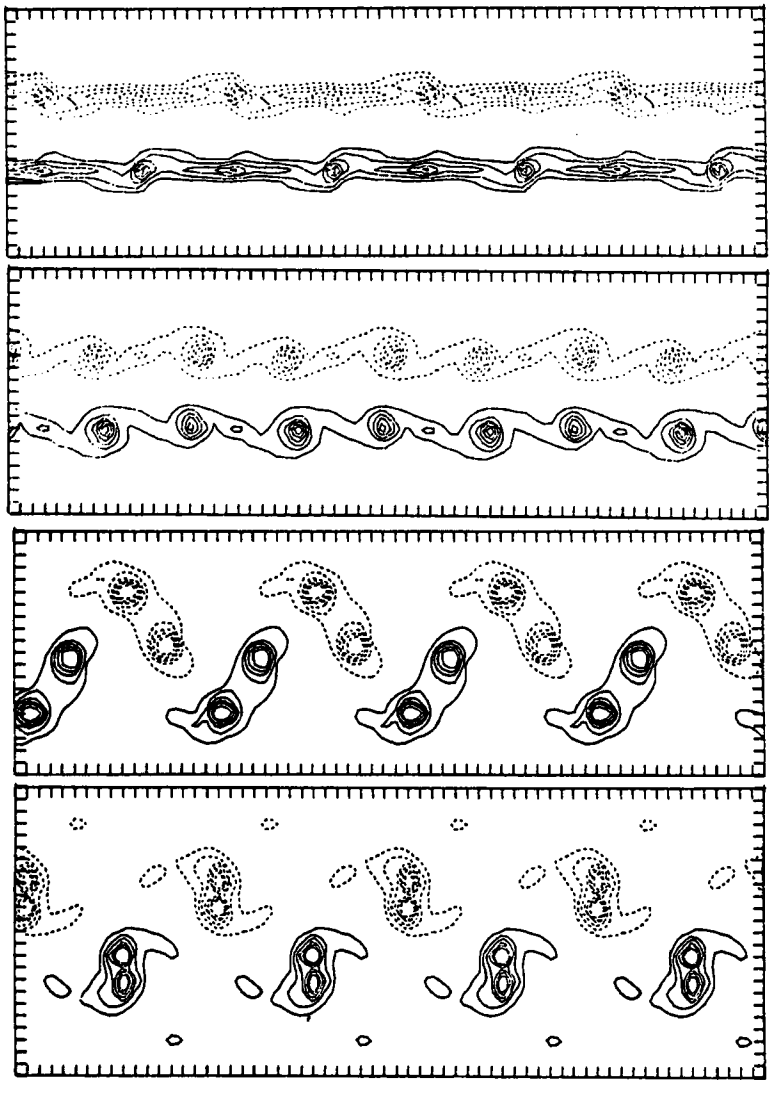

FIGURE 1. Formation of a vortex street for $h/\lambda = 0{\cdot}375$. Merging of 'secondary' vortices with 'primaries'.

have a finite thickness (Zabusky & Deem 1971).) If one is modelling a wake on the computer starting from vortex sheets, one thus has to bias the initial condition to achieve the desired staggered street configuration. A convenient initial configuration is to impose the same small-amplitude sinusoidal perturbation on both sheets. The initial state is then characterized by the ratio h/λ of sheet separation h to perturbation wavelength λ. In a real wake the value of h/λ is set by the oscillations of the boundary layers on the body, and is conveniently expressed by the dimensionless Strouhal number based on the shedding frequency. In a real experiment the Strouhal number depends on the Reynolds number, in contrast to a numerical experiment where we can vary h/λ at will.

On the basis of a series of numerical calculations, employing some 21 point vortices

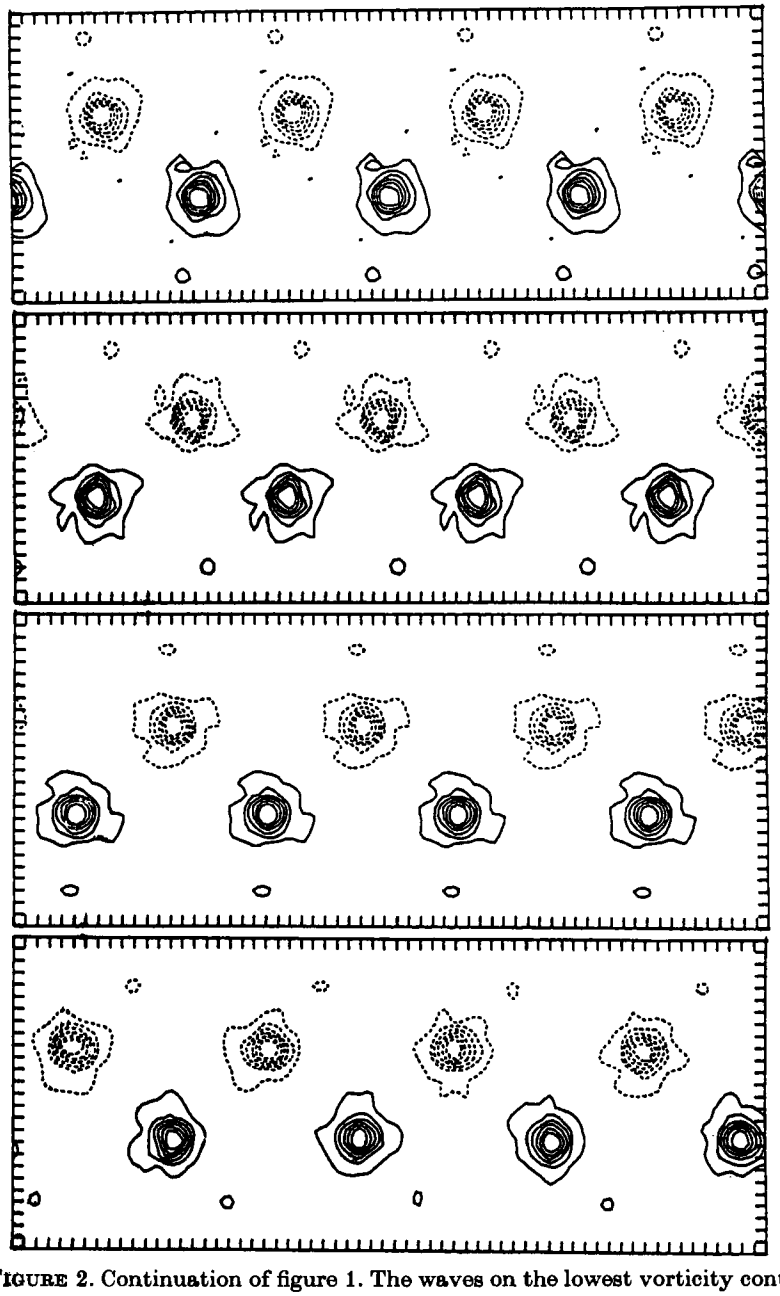

FIGURE 2. Continuation of figure 1. The waves on the lowest vorticity contour eventually get out of phase.

per wavelength as a discretization of each sheet, AK concluded: 'There appears to be a fairly general pattern followed in the formation of vortex streets from vortex rows which is independent of $[h/\lambda]$.' This conclusion is not borne out by our numerical experiments. On the contrary, it appears that there is a lower 'critical' value of h/λ below which no street is formed, and an upper 'critical' value beyond which the initially formed street undergoes a pairing within each row to a street of twice the

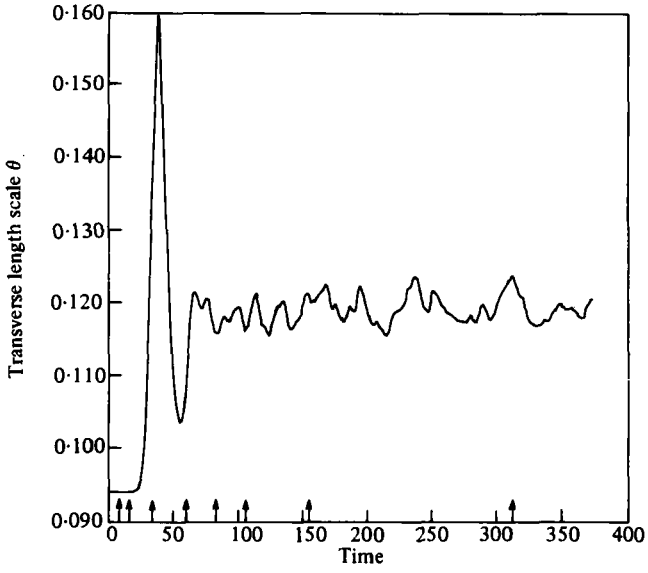

FIGURE 3. Variation of the momentum thickness θ for the 'prototype' of vortex street formation. The arrows mark the instants corresponding to the panels in figures 1–2.

longitudinal scale. Presumably several such pairings can take place in succession for large h/λ. The problem is complicated by the fact that a vortex street is not a stable configuration but rather a metastable state. Numerical errors, which resemble the background noise in a real flow, will therefore trigger instabilities of the street after a sufficiently long time.

Figures 1 and 2 present a 'prototype' of street formation. The ratio h/λ was equal to 0·375 and the figures show constant-vorticity contours at successive times. The contour levels in the top two panels of figure 1 were adjusted by the code to avoid crowding of contour lines. In all other figures in this paper the contour levels are set in the earliest panel and are unchanged for the remainder of the run. The set of levels used is always symmetrical about zero. The amplitude of the perturbation for figure 1 was one-eighth of a grid spacing. The wavelength was chosen such that four vortex blobs of either sign should emerge. Initially we see that the sheets roll up into 'primary' and 'secondary' vortices, and that the secondaries then are absorbed into the primaries. The contour plots are of course slightly misleading. In reality the vortices are concentrated along winding curves representing vortex sheets. We have previously shown examples of this for the roll-up of one vortex sheet (AS, figure 2, see also figure 18 below). Contour plots smooth out this structure. Furthermore, low-vorticity background 'debris' arising from the merging events is suppressed. We have continually checked that these shortcomings of our 'flow visualization' are not distorting our conclusions. (These checks are described at the end of this section.) For display purposes, however, we have generally found the contour plots superior to high/low intensity point plots of the vortices. The full length of the flow box is shown in the figures but not the full width (for the 64×64 grid the flow box is square, for a 512×256 grid it is rectangular with aspect ratio 2 and so on). The width is continually adjusted by the plotting routine so that only the part of the flow box that actually contains vorticity is reproduced (except for the two bottom panels in figure 10 as explained in

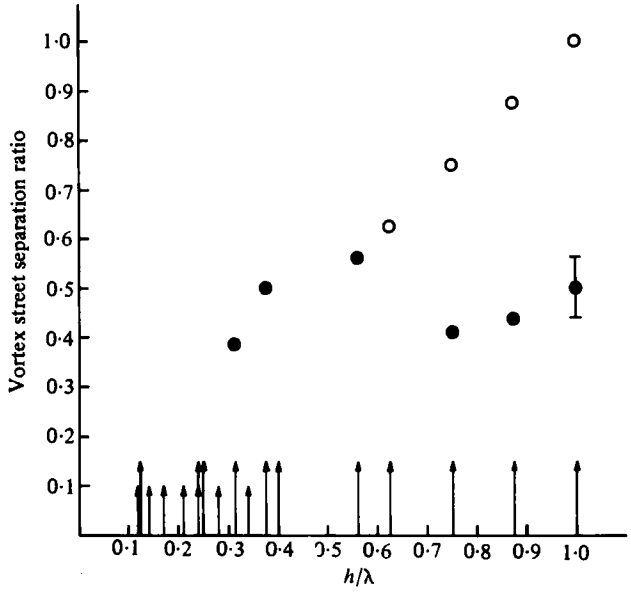

FIGURE 4. Summary of runs performed here (tall arrows) and in Abernathy & Kronauer (1962) (short arrows). Solid circles correspond to (metastable) vortex streets. Open circles correspond to streets that were unstable to a pairing within each row. An error bar appears for $h/\lambda = 1{\cdot}0$ since the street after pairing was rather irregular.

the caption for that figure). Thus the widths of individual panels in our figures are generally smaller than the distance between the rigid boundaries.

Figure 3 shows the temporal variation of the momentum thickness θ of the flow in figures 1–2. To define θ we first calculate the x-averaged longitudinal velocity $\overline{u}(y, t)$. Then

$$\theta(t) = \int dy\, \overline{u}(y,t)/\overline{u}(0,t), \tag{1}$$

where the integral on y runs from bottom to top; $y = 0$ denotes the centre-line, and we always imagine our frame of reference chosen so that the velocity vanishes far above and far below the band occupied by the vortices. The basic unit of length is chosen such that the distance between the rigid boundaries ($y = \pm 0{\cdot}5$) is unity. The arrows in figure 3 correspond to the panels shown in figures 1–2. From figure 3 we see that after the initial transient (secondary vortices merging with primaries) the width settles down to a constant value with small oscillations. At the level of contour plots these oscillations show up as waves on the outermost contours. (The related phenomenon of waves on the bounding curves of uniform vortices has been studied by Deem & Zabusky (1978) and Zabusky, Hughes & Roberts (1979) using the method of 'contour dynamics'.) Initially these waves are completely in phase along the street (top three panels of figure 2). In the bottom panel of figure 2 the waves have gotten out of phase. Shortly thereafter the street structure will begin to break down.

It is instructive to vary the ratio h/λ (as did AK) and study the influence of this parameter on the initial instability. However, we must caution the reader that laminar stability calculations with the type of code used here should not be blindly trusted (cf. Christiansen 1973 and AS). First, the vortex-in-cell method leads to a velocity anisotropy between two point vortices. Second, the imposition of a grid effectively

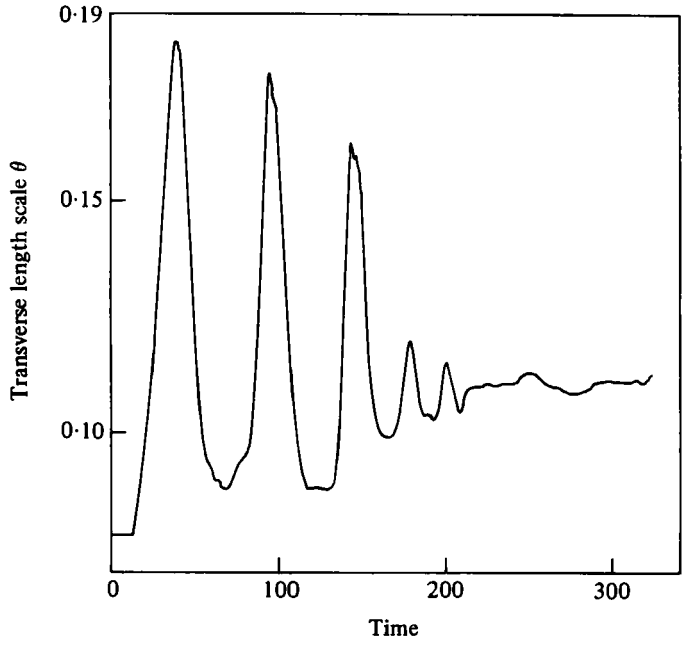

FIGURE 5. Variation of the momentum thickness θ for $h/\lambda = 0{\cdot}3125$. Note the long initial transient period compared to figure 3.

means that the vortex sheets have a finite width, i.e. there are other parameters in the problem than h and λ. We choose to present our results first and then discuss why we believe them to be trustworthy.

Figure 4 summarizes the runs performed. The initial value of h/λ is plotted along the abscissa and our runs are shown by the tall arrows. The ordinate gives the ratio of transverse to longitudinal spacing for the emerging street (if any). The range in h/λ from 0·1 to 1·0 was explored. The values of h/λ for the numerical experiments in AK are shown by short arrows. As we shall see, all but one of them fall in the range where we see *no* vortex street. To appreciate the difference between our calculations and those in AK we note that the dimensionless time variable $\Delta Ut/h$, where ΔU is the initial velocity deficit, was approximately unity where the runs in AK were terminated. In the work reported here the value of $\Delta Ut/h$ was of order 10 at the end of a run. This together with the improved spatial resolution is the main reason for the differences in our conclusions.

In the range $0{\cdot}3 \lesssim h/\lambda \lesssim 0{\cdot}6$ the vortex street formed more or less as in figures 1–2. The traces of θ *vs.* t for the two cases $h/\lambda = 0{\cdot}3125$ and $h/\lambda = 0{\cdot}563$ are shown in figure 5 and 6 respectively. For $h/\lambda = 0{\cdot}3125$ the initial transient period has become much longer than for $h/\lambda = 0{\cdot}375$ (figure 3). The secondary vortices rotate about the primaries at least three times before merging. For $h/\lambda = 0{\cdot}563$ the slow modulation of the $\theta(t)$ trace suggests an incipient instability of the wide vortex street. Both observations may be taken as precursors of the qualitative changes that take place when h/λ is either increased or decreased beyond the range $0{\cdot}3 \lesssim h/\lambda \lesssim 0{\cdot}6$. It is interesting to note that the lower limit of this range coincides approximately with the celebrated Kármán ratio, 0·281... (see Lamb 1945). This is probably entirely fortuitous, but it is the only instance where a ratio of transverse to longitudinal scale of this size appears

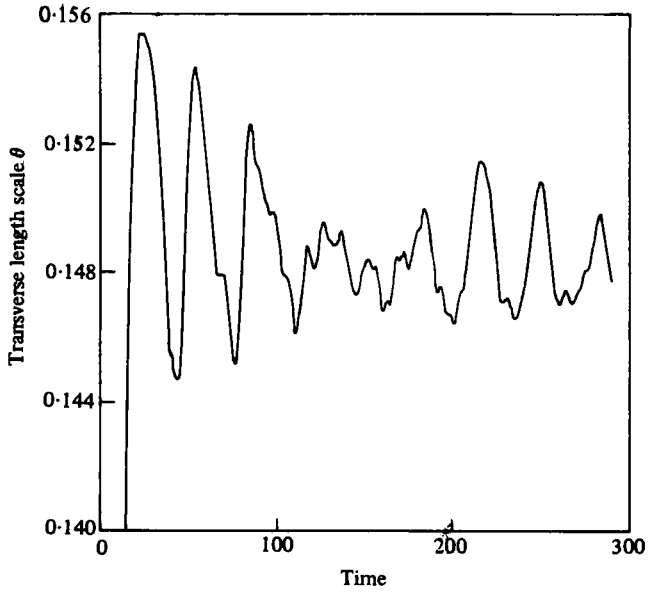

FIGURE 6. Variation of the momentum thickness θ for $h/\lambda = 0{\cdot}563$. Note the slow modulation that indicates an incipient instability.

in any significant way. The vortex streets seen in the simulation all have blob separation ratios that are 1·5–2 times larger than von Kármán's value. Of course our streets consist of finite-area vortices and not points as von Kármán assumed in his analysis. The stability problem for a vortex street with finite-size vortices is not fully understood (cf. Christiansen & Zabusky 1973; Zabusky 1977).

For runs with $h/\lambda = 0{\cdot}75, 0{\cdot}875$ and 1·0 a distinctive new mode appears. The secondary vortices, which decrease in size as the initial sheets are placed further apart, now rapidly merge with the primaries producing a street which accurately retains the values of h/λ and θ of the initial sheet configuration. As shown in figure 7 this street is unstable to a pairing motion within each row leading to a new metastable (albeit rather irregular) street with twice the longitudinal spacing. In figure 4 the initial wide street is shown by open circles, the (short-lived) paired street by solid circles. The discovery of a pairing mode is related to results obtained by Taneda (1959) who published flow-visualization pictures indicating a structural transition of this type. In the experiments, which are performed at much lower Reynolds number, the ratio of longitudinal scales of the street before and after the transition is not precisely 2 : 1 and is Reynolds-number dependent. This suggests a mode wherein the initial street structure is first entirely obliterated. The unstable wake thus produced is then unstable to the formation of a vortex street of larger scale. In terms of vortex structures it seems that in the experiments the street vortices become elongated and overlap and two wide vortex sheets result. These then roll up into the secondary vortex street. The ratio of longitudinal scales for this type of mechanism clearly need not be exactly 2 : 1. We propose that the simpler pairing process seen numerically at high Reynolds number is related to the more complex modes detected in the experiments. The occurrence of a pairing within each of the well-separated rows is furthermore natural in view of the predominance of this basic instability for an isolated shear layer (Lamb 1945; Winant & Browand 1974). Christiansen & Zabusky (1973) claimed to see the inviscid 'Taneda

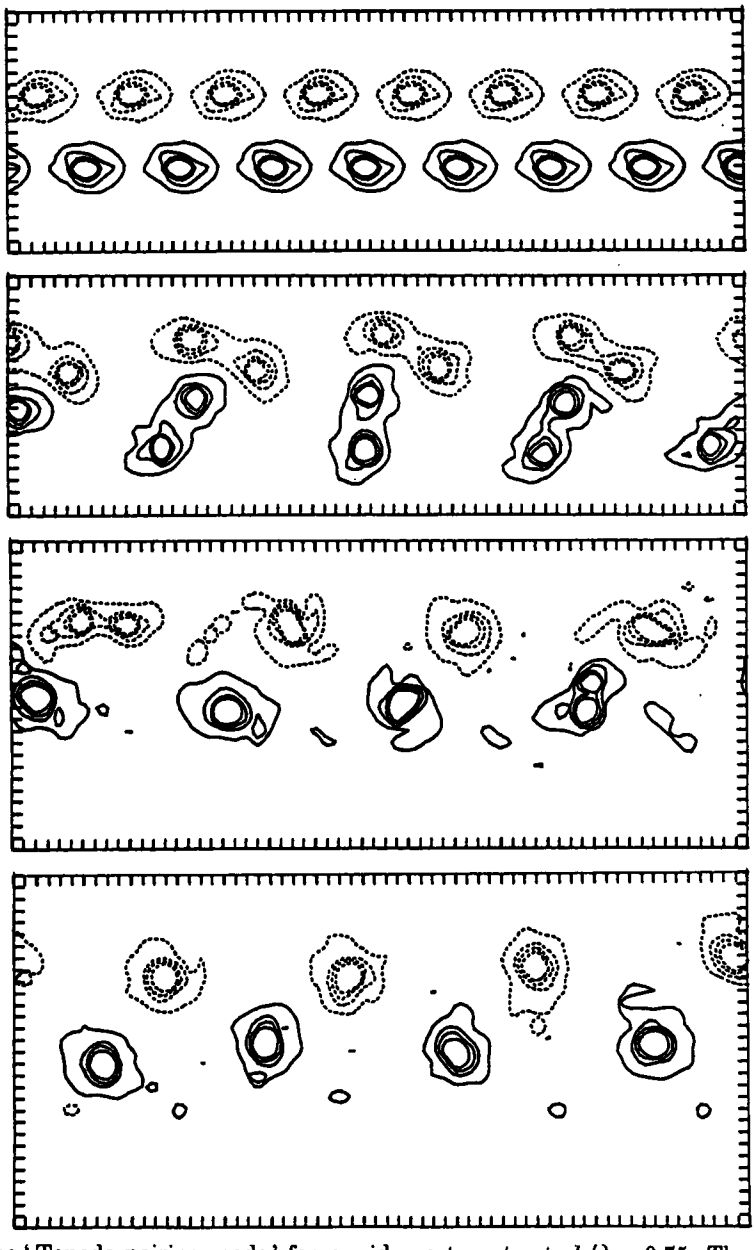

FIGURE 7. The 'Taneda pairing mode' for a wide vortex street, $h/\lambda = 0{\cdot}75$. The merging of 'secondaries' with 'primaries' (figure 1) has already taken place before the top panel. The resulting paired street is irregular and short-lived.

pairing mode' in numerical experiments similar to those performed here although their initial conditions were somewhat different. However, they considered a short segment of the street with at most four and usually only two large vortices of either sign before pairing, thus making the regularity of the street after pairing impossible to assess.

Following the enstrophy (the sum over all sites of the grid vorticity squared) as the street evolves through the pairing in figure 7 illustrates an interesting point about the

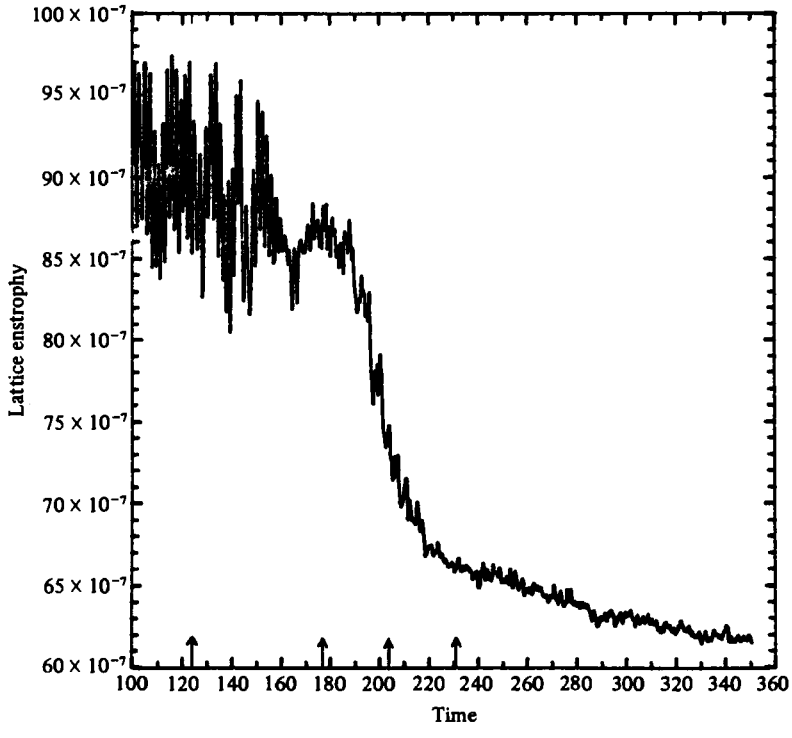

FIGURE 8. Variation of the grid enstrophy with time for the Taneda pairing. The arrows mark the instants corresponding to the panels in figure 7. Note the sharp drop in enstrophy during vortex merging.

nature of the dissipation in the vortex-in-cell algorithm. This is shown in figure 8, where the four arrows mark the times corresponding to the panels in figure 7. A sharp drop is observed in the enstrophy as the vortices pair. In the absence of coalescence vortex blobs appear to be stable entities and do not grow diffusively over the duration of our runs. The enstrophy (calculated from the grid vorticity) is constant once the initial vortex sheets roll up and the fine-scale structure within each blob has been washed out by the effects of the finite grid size and time-stepping errors. (This relaxation can be clearly seen in figure 18.) When two blobs subsequently merge, however, irrotational fluid is entrained and, when it gets pulled out into regions too fine to resolve, the enstrophy decreases. Thus our code behaves very much like a high-Reynolds-number two-dimensional fluid. An enstrophy 'cascade' (Batchelor 1969; Kraichnan 1967) only operates after the entrainment of irrotational fluid as argued in AS. Vortex merging is an 'irreversible' event; hence it is accompanied by dissipation.

At the other extreme of the h/λ range the secondary vortices are strongly influenced by the primaries of opposite sign and patterns of periodic motion ensue. An example is provided in figures 9–10 ($h/\lambda = 0{\cdot}24$) with the corresponding $\theta(t)$ trace in figure 11. The arrows in figure 11 mark the times corresponding to the panels in figures 9–10. The secondary vortices are captured by the primaries of opposite sign and transported once around. Since the dipoles formed have a small net circulation, the two rows must separate (in order to conserve momentum) and the momentum thickness increases dramatically. The cycle shown in figures 9–11 may in principle be repeated, but

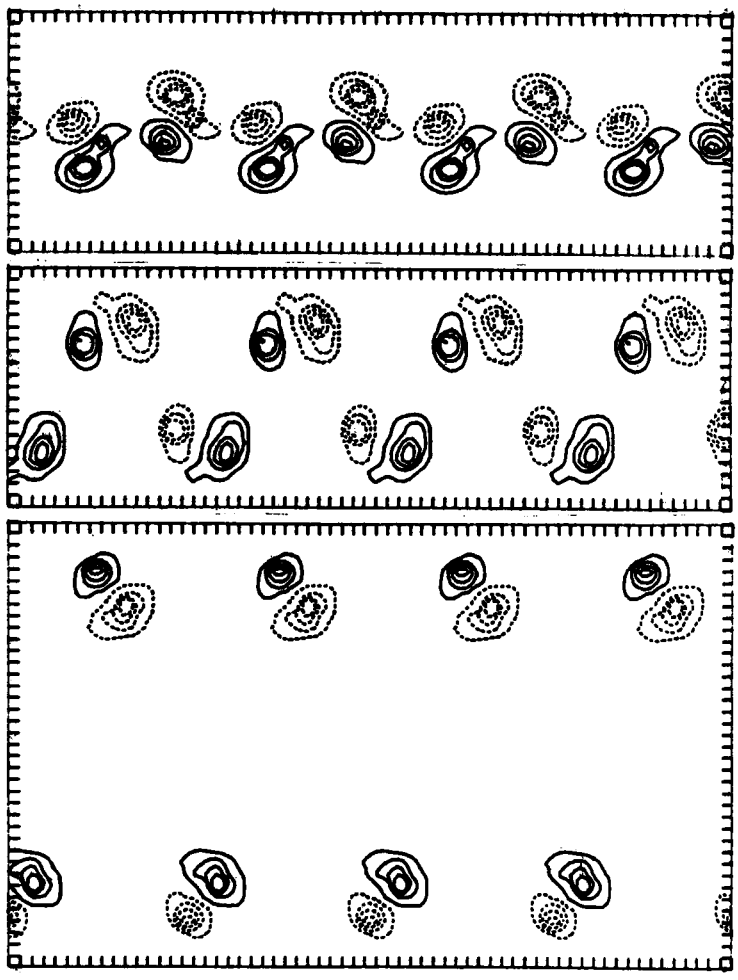

FIGURE 9. Periodic motion without street formation, $h/\lambda = 0{\cdot}24$. Here the 'secondaries' never manage to merge with the 'primaries'.

numerical errors quickly accumulate and destroy the periodicity. In practice we have only observed a fraction of the second cycle before the regularity broke down. A vortex street in the sense of figures 1–3 never emerged. For $h/\lambda = 0{\cdot}1$ the amplitude of the 'swingabout' mode has become so large that the nearly neutral pairs leaving the central region collide with the top and bottom walls of the flow box.

The numerical experiments of AK are mainly in this h/λ region, figure 4. With the wisdom of hindsight, one can actually see the initial stages of a mode like figures 9–10 in figure 5 of AK. This is encouraging because it shows that the results are not unduly influenced by the velocity anisotropy (which is of course not present in AK) or by the level of discretization (20 vortices per wavelength in AK *vs.* approximately 500 in our calculations) or by the boundary conditions (unbounded flow in the y direction in AK, rigid boundaries here). It is also clear directly from the flow pictures that effects of the velocity anisotropy must be minimal. It was shown in AS that the anisotropy is virtually absent for vortex separations of more than 2–3 grid spacings and, as the figures here show, the main vortices of the street are separated by at least 5–10 grid spacings.

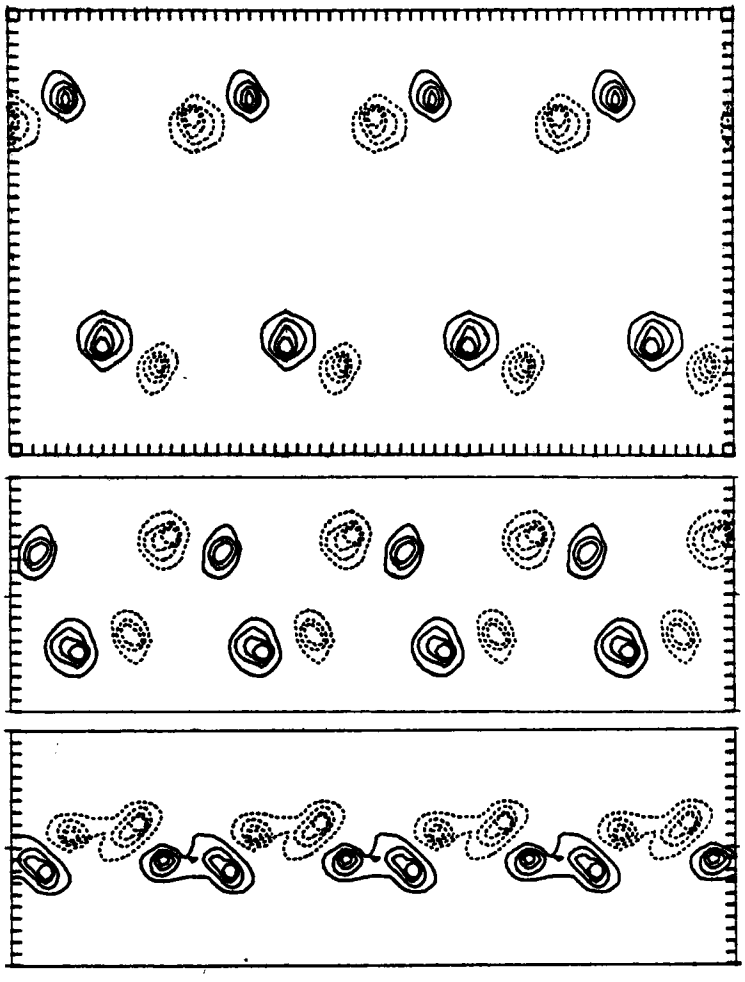

FIGURE 10. Continuation of figure 9. The bottom two panels were produced much wider by the plotting routine, indicating that vortex 'debris' was left behind (§2). The magnitude of this vorticity was less than the lowest vorticity contour level, and the panel was reduced in size for reproduction.

Except for the finite size of the flow box, the simulations should have the property of producing an identical street with all dimensions scaled by 2 if we rescale the initial configuration according to $h \to \frac{1}{2}h$ and $\lambda \to \frac{1}{2}\lambda$. Such a run was performed for the case $h/\lambda = 0{\cdot}375$, and was in fact used as the initial condition for the vortex street breakdown calculations described in §3. The resulting street may be seen in the top panel of figure 12 and it is easily verified that the street width in grid spacings is accurately one half the width in figure 2. A much larger calculation resulting in 64 street vortices of either sign (see §3) also gave the expected scaled value of the street width.

The thickness of the vortex sheets (introduced by the grid) does have a small effect on the resulting instability although this was not studied systematically. For example we have observed that *details* of the periodic motions in the small h/λ regime may vary when the same flow is time-stepped on a 64^2 and a 128^2 grid. Zabusky & Deem (1971) used a finite-difference algorithm to study the initial roll-up of two thick sheets initial-

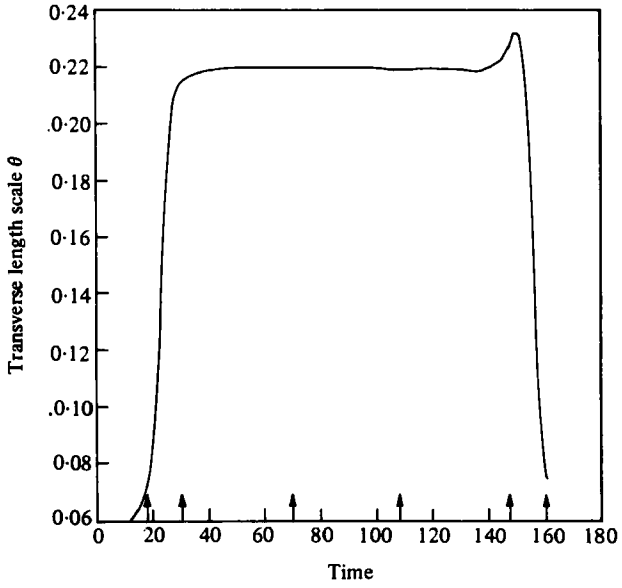

FIGURE 11. Variation of the momentum thickness θ for one period of the 'swingabout' mode. The arrows mark the instants corresponding to the panels in figures 9–10.

ized to give an approximately Gaussian velocity profile. They found the ratio of transverse to longitudinal vortex spacings to be 0·47 (as corrected by Zabusky 1977) also at least 1·5 times the von Kármán ratio and in the same range as we find with thin sheets (cf. figure 4).

To conclude this section, we return to the question of the appropriateness of vorticity contour plots as a means of flow visualization. We have monitored two quantities for the flows shown in figures 1–3 and 7–8. The first of these is a measure of the relative magnitude of the vortex 'debris' thrown off as 'arms' (cf. figure 19) during merging events. We calculated as a function of time the number of elementary point vortices of either sign that were outside the lowest contours. (This is arbitrarily called debris although some of it does in fact follow the structures in their motion.) If this number increases with time, more and more elementary vortices are being transferred from the structures to the background which, as we have noted, is suppressed by the contour plots. For the street roll-up in figures 1–3 the number of vortices in the debris constituted approximately 30 % of the total. The lowest contour corresponds to a density of about one elementary point vortex per grid square. For the Taneda pairing in figures 7–8, the debris increased to about 40 % of the total and the lowest contour was drawn slightly higher. The actual percentages are not very meaningful since they depend on our definition of the lowest contour and also on the mesh size of the underlying grid. The important thing to note, especially in the turbulent regime, is that the structures apparently persist. (We shall return to this in § 3.)

We should also point out that, although 40 per cent 'debris' may sound significant, the dynamical importance of this background vorticity is probably not so large. The reason is that the background vorticity is a mixture of point vortices of both signs. Hence the net circulation of a finite area of this debris is reduced by cancellations between oppositely signed points. Indeed, the sum over all sites of the absolute value

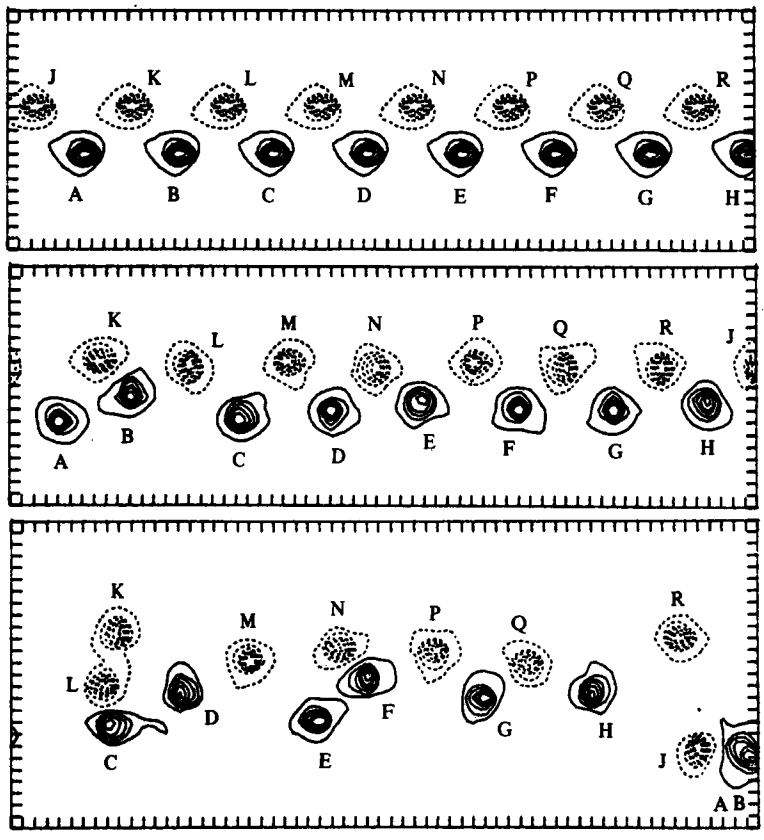

FIGURE 12. Breakdown of a vortex street for $h/\lambda = 0{\cdot}375$. The top panel is a scaled version of the street in figure 2. The vortex regions have been labelled and followed using intermediate pictures.

of the grid vorticity decreases in time due to elementary vortices of one sign being mixed into regions or structures of the opposite sign. As one would expect, considerable mixing takes place during roll-up when vortices from one sheet are advected across the midline and become wound up in the street vortices resulting from the other sheet. This effect is hard to see in a contour plot with fixed levels. For both the runs in figures 1–3 and 7–8 the relative drop in the calculated sum was only about 10 %. This number is again dependent on the mesh size of the grid. Varying the mesh size by a factor of 2 either way changes the mixing by at most one percentage point. For the background on the other hand, the sum of absolute values of grid vorticity on the 64^2 grid was approximately 20 % of the total at the end of the run. When the grid was coarsened to 32^2 this fraction dropped below 10 %, which indicates considerable mixing of opposite signed vortices in the background.

3. Breakdown of a vortex street

Figures 12–14 show the results of allowing numerical errors to accumulate in time and trigger the instability of the street. As mentioned in § 2 the street shown in the top panel of figure 12 is a scaled version of the one formed in figures 1–2. The calculation displayed in figures 12–14 is not in itself large enough to give a realistic picture of the

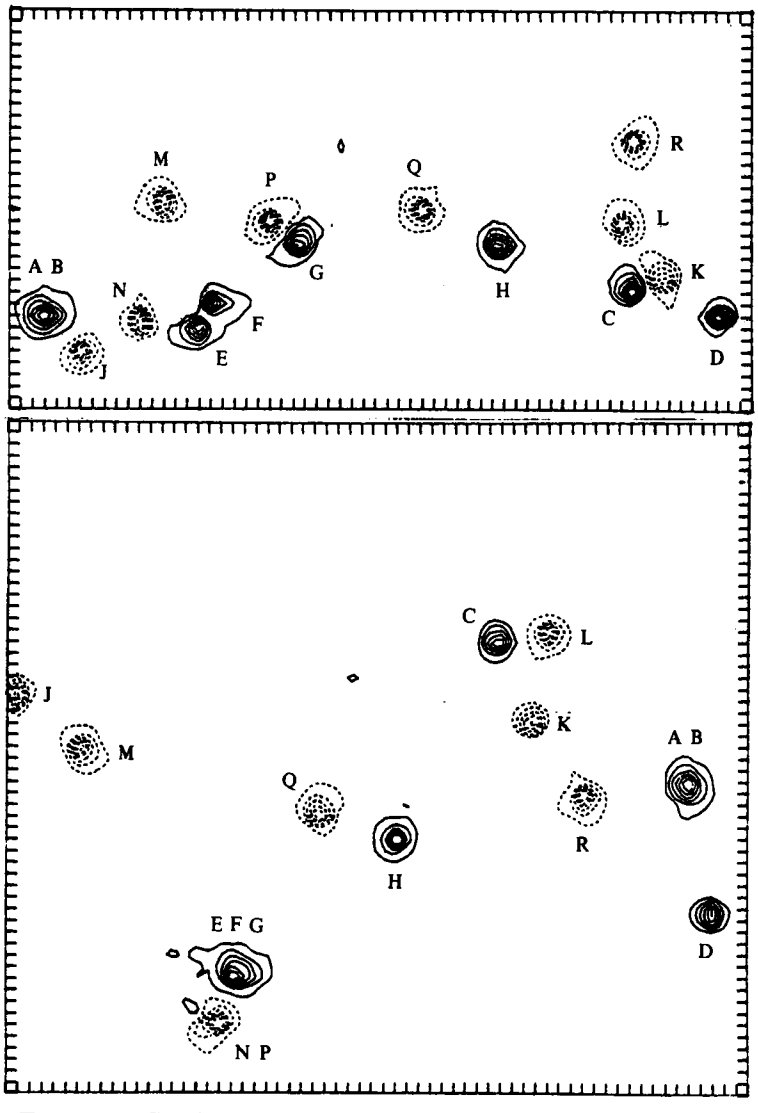

FIGURE 13. Continuation of vortex street breakdown from figure 12. Doublets, triplets and neutral pairs form.

two-dimensional turbulent shear flow that evolves. Statistics such as x-averaged profiles calculated for this flow would have little meaning in view of the small number of vortex structures within the periodic boundaries. However, these figures do bring out two essential dynamical modes that have been seen in much larger simulations. These are the merging of like-signed vortex regions, and the formation of neutral pairs (vortex dipoles) that then translate away from the central line. In figures 12–14 the vortex regions in the street were labelled A–H, J–R and, using many more pictures than we show here, their motion was tracked. In later stages of evolution we clearly see the formation of doublets (AB, NP), even a triplet (EFG), and also the escape of a neutral pair (CL).

We have performed two large simulations using 16384 vortices on a 512×256 grid.

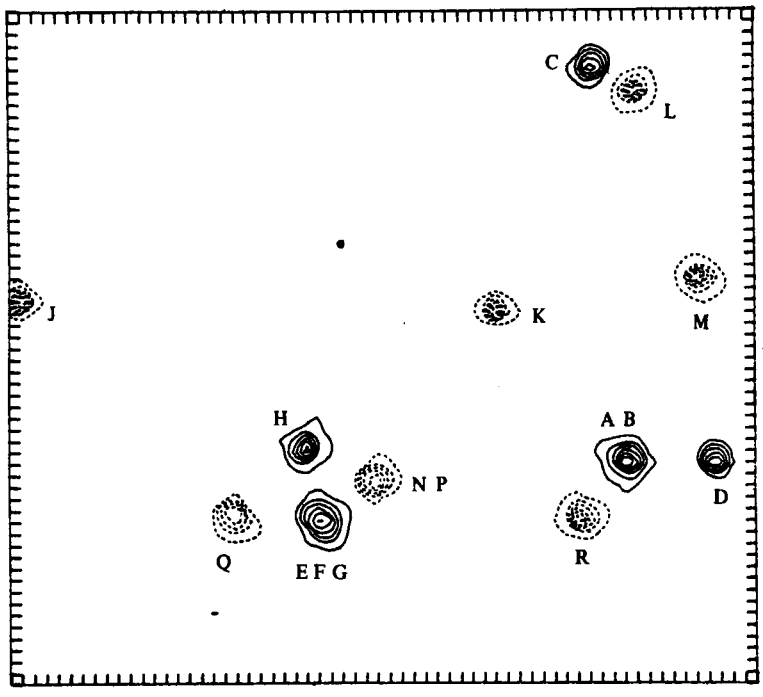

FIGURE 14. Late stages of vortex street breakdown, $\Delta Ut/h \cong 180$.

In the first of these two regularly spaced rows of identical point vortices were allowed to roll up into a vortex street with 64 finite-area vortices of either sign, a scaled version of the streets in figures 1–2 and 12. The street persisted until the dimensionless time variable $\Delta Ut/h$ (defined in § 2) had a value of the order 100. The instability which then intervened started at a specific point along the street and was for some time completely localized around that point. Eventually the disorganization spread to the left and right of the instability centre. The dynamics after breakdown was dominated by the modes exemplified in figures 12–14. Except for the amalgamation events already noted the vortex blobs from the original street persisted until the end of the simulation. It was not difficult to follow individually the 128 vortex regions as the system evolved in time. It was possible to keep track of pairings of like-signed vortices and to record as a function of time the number of doublets and triplets. Only very rarely would fractional circulations result. The accuracy with which doublets and triplets apparently acquired twice and three times the circulation of the street vortices was noteworthy. There were several instances of doublets of opposite sign which, having been formed through entirely different sequences of events, ultimately came into close contact in an otherwise vortex-free region and propagated in a straight line as a neutral pair.

In the other large simulation, we initialized two random vortex sheets of opposite sign. The constituent point vortices all had the same magnitude but their positions along the two sheets were random. The velocity deficit and the sheet separations initially had the same value as in the first large simulation. The roll-up of course did not produce a vortex street but rather two bands of finite-area vortices with random circulations. The resulting flow was similar to the previous one in that clearly identifiable structures emerged and persisted for the duration of the run. The details of the

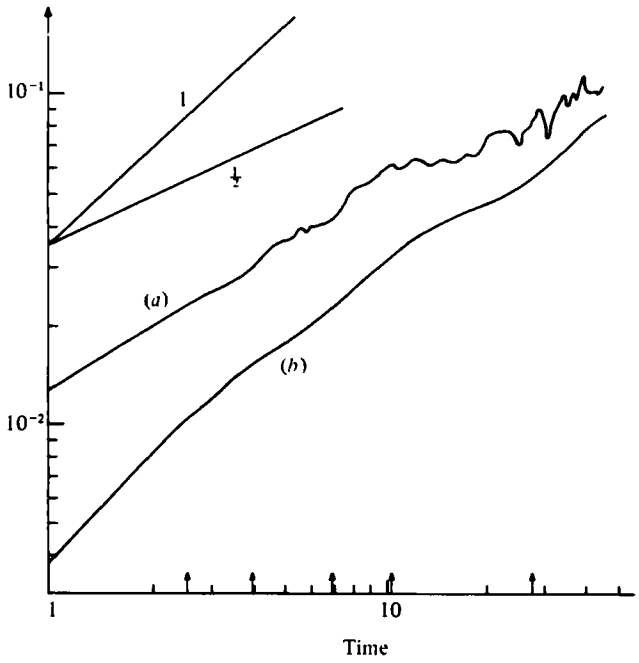

FIGURE 15. Variation of (*a*) the momentum thickness θ and (*b*) the variance of y co-ordinates of the positive vortices for the turbulent flow resulting from two random vortex sheets. The arrows correspond to the instants when $\theta/\theta_i = 2\sqrt{2}, 4, 4\sqrt{2}, 8, 8\sqrt{2}$, where θ_i is the initial momentum thickness. Time averages of scaled profiles were initiated at these times.

dynamics of these structures, however, was markedly different owing to the altered distribution of vortex blob circulations. With random initial conditions formation of neutral pairs is suppressed since the probability that two contiguous vortex regions have circulations of the same magnitude but opposite sign is very small. Merging of like-signed vortices still took place much as before but the distribution of circulations remained broad. The main impression was of a diffusively spreading assembly of finite-area vortices. The momentum thickness grew roughly as $t^{\frac{1}{2}}$ (figure 15 *a*), the variance of y co-ordinates of either positive or negative vortices grew linearly in time, figure 15 (*b*). (The significance of the arrows in figure 15 is explained later.)

A quantitative measure of the persistence of vortex structures is given by the ratio of background to total vorticity mentioned in § 2. For the illustrative run in figures 12–14 the vortices not accounted for within the lowest contour increased steadily to almost 50 % of the total number. We have already argued that the dynamical significance of the background is much less than this percentage suggests. For the street shown in the top panel of figure 12 the fraction of debris (as defined in § 2) is already 30 %. Furthermore, point plots of the vortices reveal clearly identifiable structures during the entire run. For the larger simulation at least two-thirds of the number of vortices that fell within the lowest contour level during the vortex street stage remained within that level and thus were associated with structures for the duration of the run. In particular, there were well-defined vortex structures present, containing a substantial fraction of the total vorticity, during the time when the scaling checks in figures 15–17 were performed.

The turbulent flow that results from either of the above initial conditions is traditionally expected to scale according to a set of similarity laws known as self-preservation theory (Monin & Yaglom 1971; Tennekes & Lumley 1972). For the temporal evolution of a single infinite sheet the scaling forms for profiles of x-averaged velocity, velocity fluctuation, Reynolds stress etc. may be written down at once using dimensional analysis. The only two available quantities are the velocity jump ΔU across the sheet and the time t. For example, the thickness of the unsteady shear layer that evolves, and in fact any other length scale, is predicted to grow proportionally with ΔUt. This simple scaling theory was discussed in detail in AS and its limits of validity were pointed out.

For the case of two sheets we have at our disposal three quantities: the initial velocity deficit ΔU, the initial separation of the sheets h and the time t. We choose our frame of reference such that the velocity vanishes above and below the two layers and initially equals $-\Delta U$ in between. Dimensional analysis and the assumption of a single transverse length scale implies that the x-averaged longitudinal velocity $\bar{u}(y,t)$ has the form

$$\bar{u}(y,t) = -(\Delta U)^{1-\beta}(h/t)^{\beta} f(y/\theta). \tag{2}$$

Here β is some exponent as yet undetermined, f is a universal function in principle calculable from the equations of motion and θ is the momentum thickness of the flow, defined in (1). Similar assumptions for θ imply

$$\theta = \text{const.} \times (\Delta Ut)^{\alpha} h^{1-\alpha}. \tag{3}$$

For θ actually to grow we must have $\alpha > 0$, and we shall see that the Cauchy–Schwartz inequality restricts α to $\alpha \leqslant 1$.

Conservation of linear momentum leads to the requirement that

$$\int dy\, \bar{u}(y,t) = -(\Delta U)^{1-\beta}(h/t)^{\beta}\theta \int d\eta f(\eta), \tag{4}$$

is a constant ($= -h\Delta U$). Substituting (3) and collecting powers of t, we see that $\beta = \alpha$; hence

$$\bar{u}(y,t) = -\Delta U(h/\theta) f(y/\theta) \tag{5}$$

(so that equation (1) requires $f(0) = \int d\eta f(\eta)$). Scaling of the velocity correlation function $\overline{uv}$, which equals the Reynolds stress since $\bar{v} = 0$, follows immediately from (5) and Reynolds' equation

$$\partial\bar{u}/\partial t = -\partial\overline{uv}/\partial y. \tag{6}$$

Thus,

$$\overline{uv} = \Delta U(h/t) f_{\chi}(y/\theta), \tag{7}$$

where the function f_{χ} is related to f in (5) by

$$f_{\chi}(\eta) = -\alpha\eta f(\eta). \tag{8}$$

The x-averaged kinetic-energy density,

$$\bar{e}(y,t) = \tfrac{1}{2}(\overline{u^2} + \overline{v^2}), \tag{9}$$

satisfies an equation similar to (6) for inviscid flow:

$$\partial\bar{e}/\partial t = -\partial(\overline{v(e+p)})/\partial y, \tag{10}$$

where p is the pressure divided by the (constant) density. Ignoring viscosity, the y integral of $\bar{e}$ is conserved, and the *ansatz*,

$$\bar{e}(y,t) = (\Delta U)^{2-\gamma}(h/t)^{\gamma} F(y/\theta), \tag{11}$$

leads to $\gamma = \alpha$ in complete analogy with the derivation of (5). It is natural to assume that $\overline{u^2}$ and $\overline{v^2}$ both scale in the same way as $\bar{e}$. We then have

$$\overline{u^2} = (\Delta U)^2 (h/\theta) f_{\parallel}(y/\theta), \tag{12a}$$

$$\overline{v^2} = (\Delta U)^2 (h/\theta) f_{\perp}(y/\theta), \tag{12b}$$

with two new universal functions $f_{\parallel}$ and $f_{\perp}$.

The proposed scaling theory consists of equations (3), (5), (7), (12*a*) and (*b*). It has the required properties of conserving both linear momentum and kinetic energy, and the interesting formal property of having the exponent α in equation (3) as a free parameter. In this scaling the dimensionless ratio

$$\overline{(u^2 v^2)^{\frac{1}{2}}}/\overline{u}^2 \simeq \theta, \tag{13}$$

so that the velocity fluctuations overpower the velocity deficit in the asymptotic state. Hence, the scaling theory that we propose does not lead to a statistically self-similar turbulence. In the traditional self-similar scaling of both the plane wake and the plane jet the ratio (13) is by definition of order unity. Another way of stating (13) is to note that an intrinsic Reynolds number based on the amplitude of the velocity fluctuations, $R_\lambda \equiv \theta(\overline{u^2})^{\frac{1}{2}}/\nu$, where ν is the kinematic viscosity, will increase to infinity with time, while the large-scale Reynolds number, $R = \theta\overline{u}/\nu$, remains constant. Furthermore,

$$\overline{uv}/(\overline{u^2}\,\overline{v^2})^{\frac{1}{2}} \simeq \theta/t \simeq t^{\alpha-1}, \tag{14}$$

which by the Cauchy–Schwarz inequality provides a rigorous bound of $\alpha \leqslant 1$ for the free exponent. (Self-similarity would require $\alpha = 1$.) Finally,

$$\overline{uv}/\overline{u}^2 \simeq \theta^2/t \simeq t^{2\alpha-1}, \tag{15}$$

which strongly suggests that for a turbulent flow $\alpha \geqslant 0{\cdot}5$. Otherwise the magnitude of the Reynolds stress would decay relative to the mean flow, i.e. the velocity deficit at $y = 0$. (Here self-similarity would require $\alpha = 0{\cdot}5$.)

As we have already remarked, the velocity fluctuations in a plane wake or jet in the laboratory are fully three-dimensional. Even for an arbitrarily small viscosity, energy is dissipated at a rate set by the large scales. In a two-dimensional flow, however, if we assume small-scale isotropy, the energy dissipation rate tends to zero with the viscosity since the mean square vorticity is bounded by its initial value. The conventional self-similar plane wake can legitimately be transcribed from evolution with downstream distance to evolution in time; it follows from equation (2)–(7) if we insist that the Reynolds stress scale as $\overline{u}^2(y = 0, t)$ (i.e. $\alpha = 0{\cdot}5$). Equation (12*a*) and (*b*) would of course no longer hold.

In the remainder of this section we compare statistics from the simulation started as two random sheets with the scaling theory derived above. The arguments in § 4 suggest why this case is the most favourable one for comparison with the scaling theory. In figure 16 we check the scaling relation (5) for the mean velocity. The different symbols refer to profiles at values of $\theta/\theta_i = 2\sqrt{2}, 4, 4\sqrt{2}, 8$ and $8\sqrt{2}$ where θ_i is the initial momentum thickness. As in AS, each profile is calculated as a time average started when θ/θ_i first reached one of the values listed and terminated when θ had increased by at most

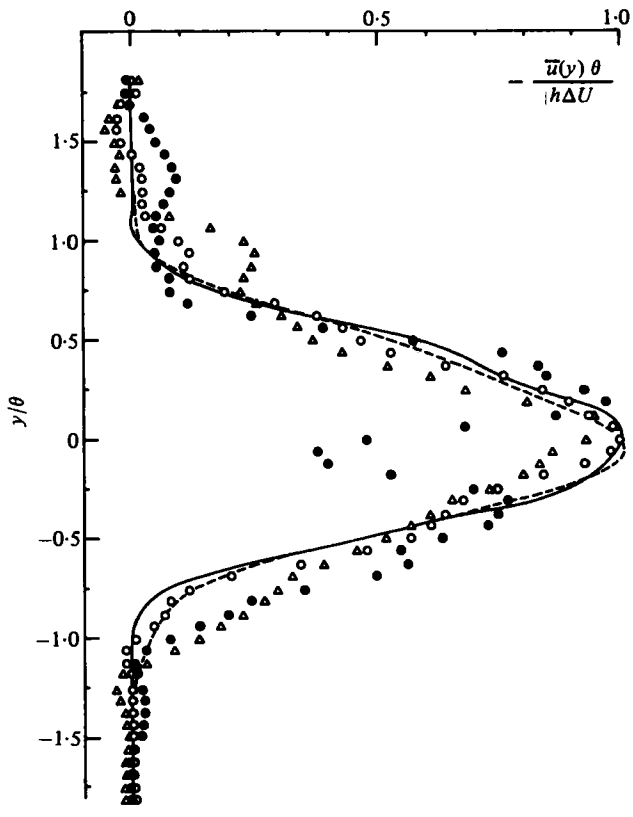

FIGURE 16. Test of the scaling relation, equation (5), for the mean velocity profile. The initial conditions were two random vortex sheets. Values of θ/θ_i are: – – –, $2\sqrt{2}$; ———, 4; ○, $4\sqrt{2}$; △, 8; ●, $8\sqrt{2}$.

25 %. The arrows in figure 15 mark when each of the time averages used for figure 16 was initiated. The agreement with equation (5) is satisfactory except for the latest time. This is reasonable both because of poorer statistics and the greater importance of boundary effects. Note that figure 16 only checks the functional form of equation (5) and not the value of the exponent α. In fact, θ need not increase as a fixed power of time for the data to collapse onto a single curve in figure 16.

In figure 17 we check the scaling prediction (12*b*). The symbols have the same meaning as in figure 16. The agreement with equation (12*b*) is satisfactory, although not nearly as good as in the corresponding plot for a single (shorter) shear layer in AS. We ascribe this to the higher level of statistical noise in the present problem due to cancellations of contributions from vortex regions of opposite sign. It should be noted that if a different power of θ were used in the prefactor in equation (12*b*) (say $1/\theta^2$ as in the self-similar, plane wake scaling) secular variations in the peak amplitudes in figure 17 would be readily apparent.

4. Discussion and conclusions

In an attempt to clarify some of the trends observed in the large simulations we have constructed and run a point vortex code that computes interactions pairwise

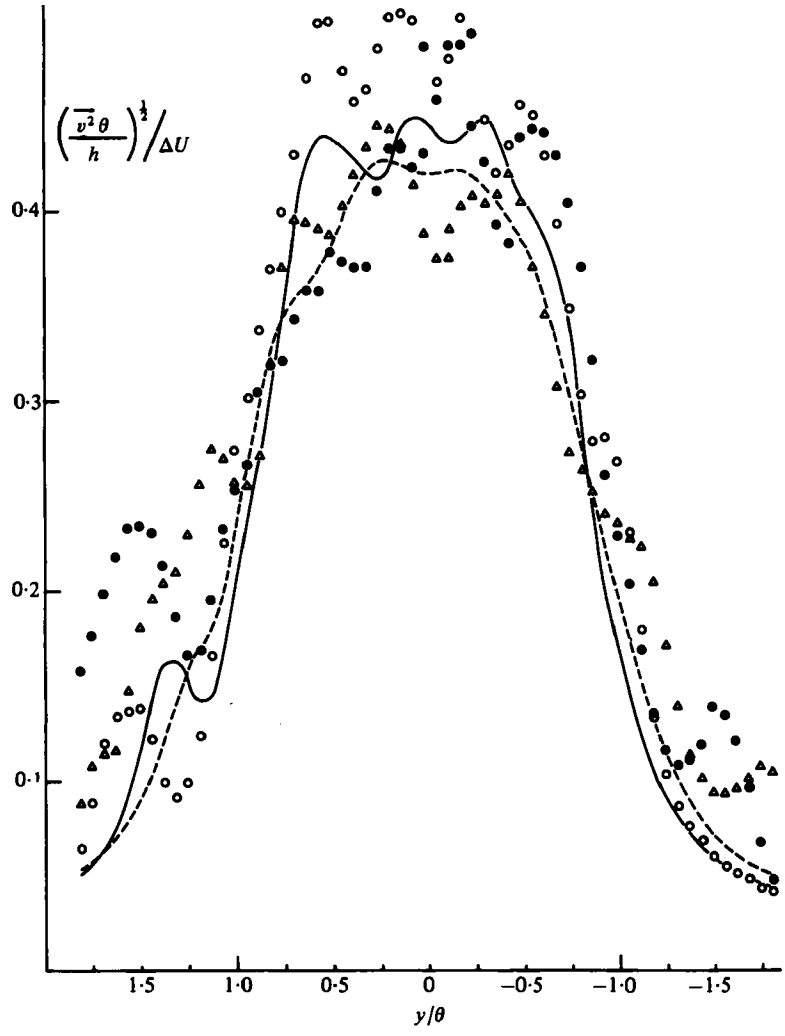

FIGURE 17. Test of the scaling relation, equation (12*b*), for the fluctuations of transverse velocity. Same initial conditions as described in figures 15 and 16. The symbols correspond to those used in figure 16.

from the exact Green's function appropriate to boundary conditions periodic in x and unbounded in y. The unit of length is now chosen equal to the horizontal repeat distance. In this representation of the full problem we are exploiting our earlier observation that the vortex blobs that form the street persist as organized entities into the turbulent regime. The merging of like-signed blobs is suppressed, although it could be incorporated by artificially amalgamating points closer to each other than some critical radius. We initialized this code from a slightly perturbed 'street' of 128 point vortices of equal magnitude (64 of either sign). After breakdown of the street there was a clear separation between a central core of randomly moving point vortices and a nearly non-interacting 'gas' of neutral pairs that were thrown off on either side of the core and propagated with constant velocity to $y = \pm\infty$. This result leads us to develop a simple kinetic theory for the evolution of this 'turbulent flow'.

If the point vortices have strengths k_j, $j = 1, \ldots, N$, the x-averaged velocity profile becomes

$$\bar{u}(y,t) = \sum_{j=1}^{N} k_j H(y_j(t) - y), \tag{16}$$

where H is the step function ($H(\eta) = 1$ if $\eta > 0$ and zero otherwise) and $y_j(t)$ is the y co-ordinate of vortex j. It follows that

$$\int dy\, \bar{u}(y,t) = \sum_j k_j y_j, \tag{17}$$

which is conserved even for periodic boundaries in x (Birkhoff & Fisher 1959), so that

$$\theta(t) = \sum_j k_j y_j(0) / \sum_j k_j H(y_j(t)). \tag{18}$$

It is clear from this expression that a neutral pair propagating outward from the centre-line does not contribute directly to the momentum thickness. To see the linearly growing scale coming from the ballistical pairs we need to measure the width of some other profile, e.g. the energy density or a scale based directly on the vorticity distribution. Thus, to resume the discussion of scaling in § 3, for breakdown of a regular vortex street we expect to see violations of equation (12*b*) in the wings of the profile. However, statistical fluctuations were so large (cf. figure 17) that a convincing scaling plot could not be produced.

By adopting a simple kinetic description it is possible to argue that not only does $\theta(t)$ not grow as fast as t, but in fact $\theta(t) \simeq t^{\frac{1}{2}}$. We start from the observation that the equations of motion also conserve the x component, $\Sigma_j k_j x_j$, of the total impulse. On the basis of the observed dissolution of the flow into a core region and a gas of vortex pairs propagating outward from the core, we split up the sum of $k_j x_j$ into two contributions, one from the core and one from the pairs. The contribution from the pairs vanishes. For a pair moving upward must have the positive vortex on the left and the negative vortex on the right, whence $\Delta x < 0$. Similarly $\Delta x > 0$ for a pair moving downward. On average we expect cancellation by symmetry. Thus the total x-impulse is carried by those vortices that remain in the core region. Let their number be $n_c(t)$. If the r.m.s. separation between neighbours in the core is denoted d_{rms} we have

$$\sum_j k_j x_j = (\sum_j k_j x_j)_{\mathrm{core}} \simeq n_c d_{\mathrm{rms}}, \tag{19}$$

or

$$d_{\mathrm{rms}} \simeq n_c^{-1}. \tag{20}$$

Next, we write down for n_c a kinetic equation in a 'relaxation time approximation', viz.

$$\partial n_c / \partial t = -n_c/\tau. \tag{21}$$

The time constant τ must be a typical time scale for motions within the core region, i.e.

$$1/\tau \simeq k/d_{\mathrm{rms}}^2 \simeq n_c^2, \tag{22}$$

where k is some average magnitude of vortex strengths. Now from (21)

$$\partial n_c / \partial t = -\gamma n_c^3 \tag{23}$$

where γ is a constant parameter. Equation (23) has the asymptotic power-law solution

$$n_c(t) \sim (2\gamma t)^{-\frac{1}{2}}. \tag{24}$$

To complete the argument we split the y impulse, equation (17), into core and pair contributions. Again by symmetry, this time of the angular distribution for the emitted pairs in either half-space, the pair contribution vanishes on average. Hence, identifying θ with the average spread in y co-ordinate of the core vortices (cf. equation (18)),

$$(\sum_j k_j y_j)_{\text{core}} \simeq k n_c \theta = \text{const.}, \tag{25}$$

which with (24) gives

$$\theta \simeq t^{\frac{1}{2}}. \tag{26}$$

This result is consistent with (20) because the average x separation of core vortices used to estimate d_{rms} is seen to scale with the same power of t as the average y separation.

The correct growth exponent for θ for breakdown of a street of point vortices all of the same magnitude need not be precisely 0·5 since the derivation given above was obviously rather crude. Let us mention just one source of error: In deriving equation (26) we used two statistical symmetries. The first of these (symmetry between pairs emitted upwards and downwards) is exact. The second symmetry (equal number of pairs emitted upward at an angle v and at an angle $-v$ to the vertical) is not necessarily true. In fact the direction singled out by the velocity deficit breaks this symmetry. Hence equation (25) is only an approximation. However, we expect the precise value of the growth exponent to provide an upper bound for the growth rate of vortex streets with distributed vortices. The reason is that finite-area vortices of like sign may merge and that reduces the probability of pair formation. Consequently n_c decays more slowly for a street of distributed vortices, and this would be reflected in a slower growth of θ.

An interesting inadequacy of the derivation of equation (26) relates to the question of distinguishing 'wake' from 'jet'. This problem arises since at the level of two parallel vortex sheets a 'wake' may be transformed into a jet-like flow by applying a Galilean transformation that compensates for the uniform mean stream. Going back to equation (19) we see that the case

$$\sum_j k_j x_j = 0 \tag{27}$$

merits special consideration. If we perturb the two sheets so that the discrete symmetry

$$\zeta(x, y) = -\zeta(x, -y) \tag{28}$$

for the vorticity ζ is *not* broken, the equations of motion will preserve it for all future times. One sheet will now evolve as the image of the other in the line $y = 0$, i.e. this line could be replaced by a solid surface. Thus it is clear that no vortex of either sign can cross the midline and in particular no neutral pairs can escape the core. The only remaining process for thickening of the layer then is the merging of like-signed vortices as in a single shear layer. Crudely speaking this leads to θ increasing linearly in time.

Figures 18–19 show the evolution of two regular vortex rows perturbed with a sinusoid that respects the symmetry (28). Since the vortices of opposite sign do not mix at all, point plots are used. In the top two panels of figure 18 the two sheets roll up into spirals. As the flow evolves the fine-scale features of the spiral arms are washed

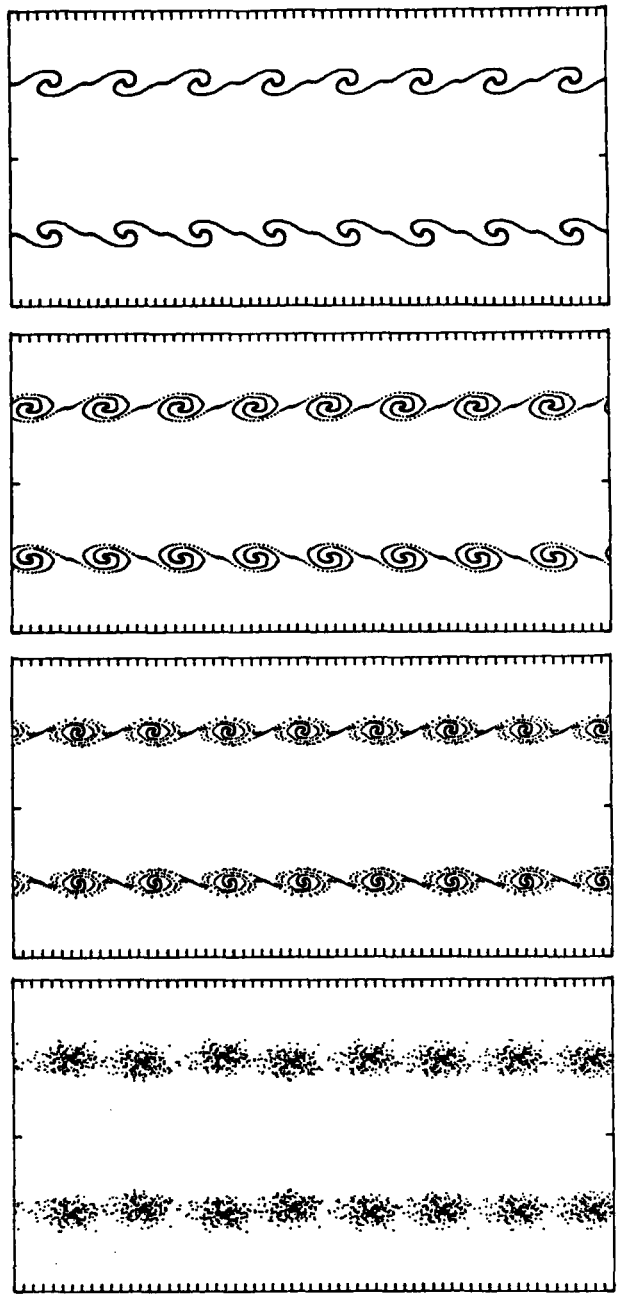

FIGURE 18. Evolution of two vortex sheets with an initial perturbation to resemble a plane jet. Point plots of vortices are used. The roll-up into spirals and the gradual obliteration of the spiral arms is shown.

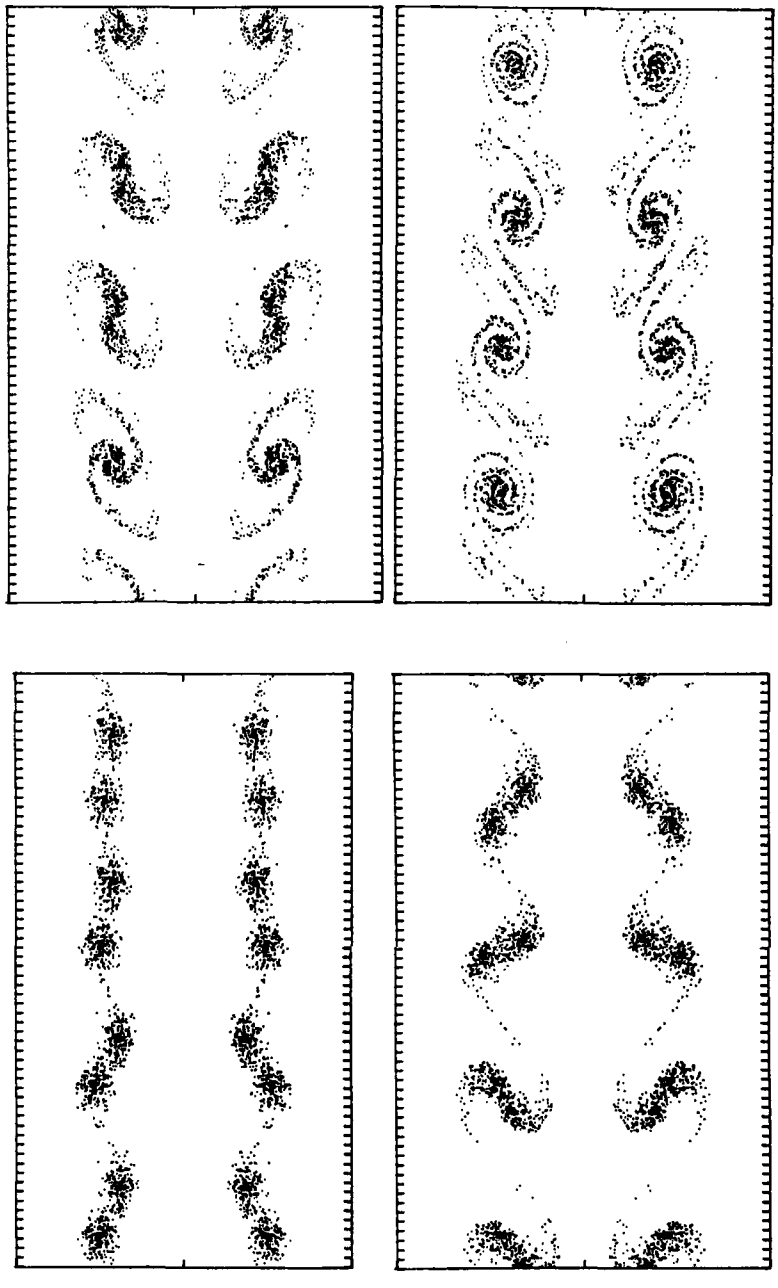

FIGURE 19. Continuation of figure 18. The two rows of finite-area vortices become unstable to a pairing mode and nearest neighbours merge.

out. By the time the pairing instability between like-signed vortex regions begins (bottom panel in figure 18) the spiral structure has been obliterated. The pairing proceeds (figure 19) and reduces the number of vortex blobs in each row from eight to four. Spiral structure is recreated on a larger scale by the vortex pairing. One more pairing was observed before numerical errors accumulated and broke the symmetry, equation (28).

It should be apparent that when a two-dimensional wake or jet is modelled numerically as an initial-value problem in a horizontally periodic box the only way to distinguish the two flows is through the symmetry of the initial instability. The conventional vortex street configuration results from an asymmetric shedding process commonly observed in the wake of a cylindrical body. The symmetrical street (figures 18–19) on the other hand has been observed in plane jets (Beavers & Wilson 1970) and the three-dimensional analogue is observed in an axisymmetric jet. The symmetry, equation (28), may then influence the subsequent evolution by favouring or suppressing certain dynamical modes. Thus we see pair emission in our two-dimensional wake, but, assuming noise did not destroy the symmetry, we would only expect to see vortex pairings in the jet (cf. Crow & Champagne 1971). We have argued that as a result the momentum thickness will increase as $t^{\frac{1}{2}}$ in the first case and as t in the second. We do not believe (as suggested by Zabusky & Deem, 1971) that the details of the initial vorticity profile (i.e. the explicit form of the profile $\zeta(y)$ at $t = 0$) constitutes a valid distinction between jet and wake in the context of two-dimensional, numerical simulations. Any profile that is perturbed in the direction of a vortex street will evolve ultimately into a turbulent wake. The initial vorticity profile may influence the vorticity distribution within individual blobs, but it is hard to see from our results why (assuming minimal universality) it would affect the scaling behaviour of the turbulent flow.

If the initial vortex regions have a broad distribution of strengths the derivation given above is not relevant. This situation arises when we follow the roll-up of two random vortex sheets of opposite sign. The probability of forming neutral pairs is now virtually zero and there is no basis for splitting up the components of the impulse into core and pair contributions. As mentioned in § 1, it is tempting to infer a breakdown of universality in the traditional sense. It is easy to set up two pairs of vortex rows, one pair regularly spaced with a sinusoidal perturbation, the other random but with the same separation and initial velocity deficit. The two turbulent shear flows that ultimately result will thicken in fundamentally different ways because of the importance of pair formation in the first case and its absence in the second. For the breakdown of a street we expect two length scales to be necessary for scaling of the large-scale statistics. For the random sheet initial condition the scaling theory of § 3 seems adequate.

The possibility that two-dimensional turbulence is non-universal was already discussed by Kraichnan (1967) for the isotropic case. Recently Delcourt & Brown (1979) suggested on the basis of numerical experiments that the growth rate of a two-dimensional shear layer depends sensitively on the distribution of circulation per unit length of the layer. Whether this dependence leads to a breakdown of universality or just to very long relaxation times could not be unambiguously decided. In the case studied here, which we shall refer to as the two-dimensional wake, however, the growth rate of the momentum thickness can be linked directly to the presence or absence of a distinct dynamical process. It appears therefore that this flow provides the most

promising testing ground for the idea of universality (in two-dimensional turbulence). We believe on the basis of our numerical experiments that the asymptotic statistical state of the two-dimensional wake depends on the distribution of circulation integrals or equivalently on some of the higher-order vorticity correlations. This question probably cannot be completely settled by performing ever larger numerical simulations, although a vortex code which retains the circulation integrals is the appropriate type of code for addressing it. In particular, one may argue that the emission of neutral pairs is only transient and will come to an end as soon as the merging of like-signed vortex regions has been operative for some time. In this argument a broad distribution of circulations will then ensue for both the street and random sheet initial conditions and the same asymptotic state will be reached. We hope the results reported here will stimulate analytical work on the problem.

We would like to thank Professor John L. Lumley for a very useful discussion of scaling and self-similarity of turbulent shear flows. We also want to thank Professors A. J. Chorin, S. K. F. Karlsson, M. V. Morkovin and S. Taneda for their comments on the manuscript. This work was made possible by a direct grant of computer time on the CRAY-1 computer at NCAR and was supported by NSF grant ATM-78-16411. H. A. would like to acknowledge the support of a Cornell Graduate Fellowship during the initial stages of this work. NCAR is supported by the National Science Foundation.

REFERENCES

ABERNATHY, F. H. & KRONAUER, R. E. 1962 The formation of vortex streets. *J. Fluid Mech.* **13**, 1–20.

AREF, H. & SIGGIA, E. D. 1980 Vortex dynamics of the two-dimensional turbulent shear layer. *J. Fluid Mech.* **100**, 705–737.

ASHURST, W. T. 1979 Numerical simulation of turbulent mixing layers via vortex dynamics. In *Turbulent Shear Flows I* (ed. F. Durst, B. E. Launder, F. W. Schmidt & J. H. Whitelaw), pp. 402–413. Springer.

BATCHELOR, G. K. 1969 Computation of the energy spectrum in homogeneous two-dimensional turbulence. *Phys. Fluids Suppl.* **12**, II 233–239.

BEARMAN, P. W. & GRAHAM, J. M. R. 1980 Vortex shedding from bluff bodies in oscillatory flow: A report on Euromech 119. *J. Fluid Mech.* **99**, 225–245.

BEAVERS, G. S. & WILSON, T. A. 1970 Vortex growth in jets. *J. Fluid Mech.* **44**, 97–112.

BIRKHOFF, G. & FISHER, J. 1959 Do vortex sheets roll up? *Rend. del Circ. Mat. Palermo* **8**, 77–90.

CHORIN, A. J. 1973 Numerical study of slightly viscous flow. *J. Fluid Mech.* **57**, 785–796.

CHORIN, A. J. 1980 Vortex models and boundary layer instability. *SIAM J. Sci. Stat. Comput.* **1**, 1–21.

CHRISTIANSEN, J. P. 1973 Numerical simulation of hydrodynamics by the method of point vortices. *J. Comp. Phys.* **13**, 363–379.

CHRISTIANSEN, J. P. & ZABUSKY, N. J. 1973 Instability, coalescence and fission of finite-area vortex structures. *J. Fluid Mech.* **61**, 219–243.

CLEMENTS, R. R. & MAULL, D. J. 1975 The representation of sheets of vorticity by discrete vortices. *Prog. Aero. Sci.* **16**, 129–146.

CROW, S. C. & CHAMPAGNE, F. H. 1971 Orderly structure in jet turbulence. *J. Fluid Mech.* **48**, 547–591.

DEEM, G. S. & ZABUSKY, N. J. 1978 Vortex waves: Stationary V-states, interactions, recurrence and breaking. *Phys. Rev. Lett.* **40**, 859–862.

DELCOURT, B. A. G. & BROWN, G. L. 1979 The evolution and emerging structure of a vortex sheet in an inviscid and viscous fluid modelled by a point vortex method. *2nd Symp. on Turbulent Shear Flows, Imperial College, London*, p. 14.35.

DURGIN, W. W. & KARLSSON, S. K. F. 1971 On the phenomenon of vortex street breakdown. *J. Fluid Mech.* **48**, 507–527.

KRAICHNAN, R. H. 1967 Inertial ranges in two-dimensional turbulence. *Phys. Fluids* **10**, 1417–1423.

LAMB, H. 1945 *Hydrodynamics*, 6th edn. Dover.

LEONARD, A. 1980 Vortex methods for flow simulation. *J. Comp. Phys.* **37**, 289–335.

MONIN, A. S. & YAGLOM, A. M. 1971 *Statistical Fluid Mechanics*, vol. 1 (ed. J. L. Lumley). Massachusetts Institute of Technology Press.

PAPAILIOU, D. D. & LYKOUDIS, P. S. 1974 Turbulent vortex streets and the entrainment mechanism of the turbulent wake. *J. Fluid Mech.* **62**, 11–31.

ROSHKO, A. 1954 On the development of turbulent wakes from vortex streets. *N.A.C.A. Rep.* 1191.

ROSHKO, A. 1961 Experiments on the flow past a circular cylinder at very high Reynolds number. *J. Fluid Mech.* **60**, 345–356.

TANEDA, S. 1959 Downstream development of the wakes behind cylinders. *J. Phys. Soc. Japan* **14**, 843–848.

TENNEKES, H. & LUMLEY, J. L. 1972 *A First Course in Turbulence*. Massachusetts Institute of Technology Press.

WINANT, C. D. & BROWAND, F. K. 1974 Vortex pairing: the mechanism of turbulent mixing layer growth at moderate Reynolds number. *J. Fluid Mech.* **63**, 237–255.

ZABUSKY, N. J. 1977 Coherent structures in fluid dynamics. In *The Significance of Nonlinearity in the Natural Sciences*, pp. 145–205. Plenum.

ZABUSKY, N. J., & DEEM, G. S. 1971 Dynamical evolution of two-dimensional unstable shear flows. *J. Fluid Mech.* **47**, 353–379.

ZABUSKY, N. J. HUGHES, M. H. & ROBERTS, K. V. 1979 Contour dynamics for the Euler equations in two dimensions. *J. Comp. Phys.* **30**, 96–106.